Bioresource Technology 435 (2025) 132882

Contents lists available at ScienceDirect

Bioresource Technology

journal homepage: www.elsevier.com/locate/biortech

Iterative enhancement of cutinase thermostability by multiple strategies based on combined directed evolution and computationally assisted design

Shiheng Chen [a,c], Lei Wang [a,c], Demin Kong [a,c], Zhisheng Wei [a,c], Xiaoqi Ling [d], Zhaohong Deng [d], Fengshan Zhang [b], Lingqia Su [a,c], Zhanzhi Liu [a,b,c], Jing Wu [a,b,c], Sheng Chen [a,c,*]

[a] Key Laboratory of Industrial Biotechnology, Ministry of Education and School of Biotechnology, Jiangnan University, 1800 Lihu Avenue, Wuxi 214122, China
[b] Shandong Huatai Paper Co., Ltd. and Shandong Yellow Triangle Biotechnology Industry Research Institute Co. Ltd, Dongying 257335, China
[c] State Key Laboratory of Food Science and Resources, Jiangnan University, 1800 Lihu Avenue, Wuxi 214122, China
[d] The School of Artificial Intelligence and Computer Science, Jiangnan University, Wuxi 214122, China

HIGHLIGHTS

- Iterative protein engineering integrating three synergistic strategies significantly enhanced the thermostability of HiC.
- Half-life of M8 at 65 °C and 70 °C increased by 8110- and 3982-fold, respectively.
- M8 exhibited superior alkaline tolerance and optimized kinetic parameters.
- Molecular dynamics simulations and structural analyses revealed stabilization mechanisms.

GRAPHICAL ABSTRACT

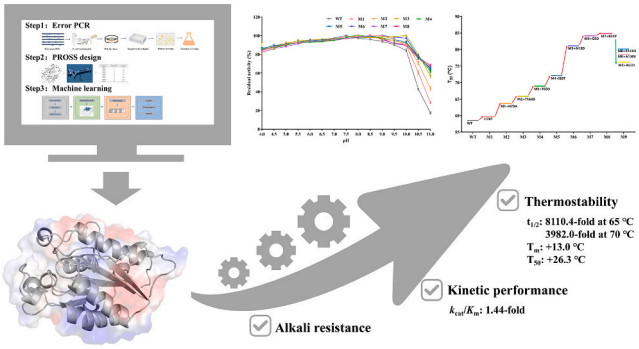

ARTICLE INFO

Keywords:
Humicola insolens cutinase (HiC)
Multi-strategy combination
Thermostability
Iterative combination
Molecular dynamics simulation

ABSTRACT

Cutinase exhibits versatile biocatalytic potential in polymer degradation, textile processing, and industrial biocatalysis, where enhancing the thermal stability under extreme conditions is essential for practical applications. To enhance the thermal stability of *Humicola insolens* cutinase (HiC), a combination of strategies approach integrating error-prone PCR, computational design, and machine learning were implemented. Through systematic iterative recombination, an octuple mutant (M8) was developed with thermal tolerance and preserved catalytic activity. The engineered mutant demonstrated exceptional stability enhancements, exhibiting 8110- and 3982-fold increases in half-life at 65 °C and 70 °C, respectively, compared with wild-type HiC. Differential scanning calorimetry revealed a 13.0 °C elevation in melting temperature (T_m), while thermal inactivation analysis showed a 26.2 °C improvement in T (temperature causing 50 % activity loss in 60 min). Notably, M8 retained full activity at standard assay temperature and exhibited a broad pH profile despite incorporating eight stabilizing mutations. Molecular dynamics simulations and structural analyses revealed that the redistribution of surface electrostatic charges and a more compact overall structure were key factors in enhancing thermal stability. In summary, this study established a framework for rational thermostabilization of cutinases while providing molecular level insights into thermal adaptation mechanisms, with methodological implications for

* Corresponding author at: State Key Laboratory of Food Science and Technology, Jiangnan University, 1800 Lihu Avenue, Wuxi, Jiangsu 214122, China.
E-mail address: chensheng@jiangnan.edu.cn (S. Chen).

https://doi.org/10.1016/j.biortech.2025.132882
Received 7 March 2025; Received in revised form 23 May 2025; Accepted 22 June 2025
Available online 23 June 2025

α/β-hydrolase family enzyme optimization. The engineered HiC mutant present significant potential for industrial processes requiring high-temperature operations.

1. Introduction

Cutinases (EC 3.1.1.74), classified within the α/β hydrolase superfamily, are low-molecular-weight biocatalysts specialized in hydrolyzing the waxy polyester cutin into fatty acids. These enzymes demonstrated broad substrate promiscuity, efficiently degrading synthetic polyesters, insoluble triacylglycerols, and low-molecular-weight soluble esters alongside their native substrate (Chen et al., 2013). Notably, cutinases demonstrated catalytic activity in esterification and transesterification reactions, supporting applications spanning detergent formulation, food processing, bioremediation, and textile/pulp-paper industries (Chen et al., 2007; Dutta et al., 2009; Hong et al., 2017).

The expanding reliance on recycled fibers in modern papermaking introduces critical technical challenges, particularly regarding adhesive contamination. Pressure-sensitive adhesives and ester-rich polyesters form sticky deposits during the recycling process. Subsequently, these contaminant residues can damage paper quality metrics and manufacturing continuity (Zhang et al., 2016). Enzymatic mitigation strategies employing cutinases address the challenge through targeted hydrolysis of ester linkages in polyvinyl acetate/polyacrylate adhesives, effectively reducing polymer molecular weight and interfacial adhesion (Hong et al., 2019). However, prolonged thermal exposure in industrial papermaking processes induces enzyme denaturation, which significantly reduces catalytic efficiency (Liu et al., 2012). Consequently, protein engineering initiatives focusing on thermotolerance enhancement emerge as an essential prerequisite for bridging this implementation gap, representing a critical pathway toward sustainable enzymatic solutions in circular paper economies.

Multiple strategies have been employed to enhance protein stability, with conventional approaches encompassing directed evolution, semi-rational design, and rational design methodologies (Xu et al., 2019). Recently, advancements in computational methods have facilitated the application of free-energy calculations and phylogenetic analysis for protein design, focusing on identifying mutants with enhanced stability compared with wild type (WT) sequences. Among the numerous computational algorithms available, Fireprot (Musil et al., 2017), PROSS (Goldenzweig et al., 2016), B-FITTER (Reetz and Carballeira, 2007), Consensus Finder (Jones et al., 2020), Rosetta Design (Liu and Kuhlman, 2006), and PopMusic (Yves et al., 2011) are widely recognized. With the advancements in the accuracy and reliability of current computational methods, prediction precision can be enhanced through artificial intelligence or machine learning to eliminate unstable mutations. This could allow computational design strategies to develop more effectively in improving protein thermal stability and catalytic activity. Each strategy has its own advantages and limitations, making the selection of the most suitable approach a critical priority.

Currently, several molecular modification strategies have been reported to improve the stability and catalytic performance of cutinase. Masayuki Oda et al. engineered a mutant by substituting disulfide bonds for the Ca^{2+} binding site and modifying the protein surface to enhance activity and thermal stability. The mutant exhibited an increase in PET degradation rate from 16 % to 33 %, with T_m values of 68.4 °C and 85.7 °C for WT and mutant, respectively (Oda et al., 2018). Additionally, Akihiko Nakamura et al. redesigned PET2 through rational surface charge modification and disulfide bond addition, generating mutant PET2-7M. The results demonstrated that the T_m value of the mutant was elevated by 6.7 °C relative to WT. Moreover, the release of PET degradation products increased from 2.4 μM to 7.8 μM. Structural analysis revealed that the enhanced thermal stability may be attributed to multiple factors including surface charge redistribution, increased α-helical content, and reduced flexibility in loop regions (Nakamura et al., 2021). Hyeoncheol Francis Son et al. employed *Is*PETase structural information to devise a rational protein engineering strategy, identifying a mutant with improved stability and degradation efficiency. The mutant exhibited an 8.8 °C increase in T_m and demonstrated 14-fold higher PET degradation activity at 40 °C compared with the native *Is*PETase. Structural analysis indicated that enhanced thermal stability correlated with additional hydrogen bonds and optimized hydrophobic interactions in the mutant (Son et al., 2019). Yinglu Cui et al. developed a computational strategy to enhance the stability and functional robustness of PETase. Through computational design and systematic clustering analysis, they redesigned a mutant, DuraPETase, which exhibited a T_m increase of 31 °C compared with the native enzyme. Moreover, DuraPETase demonstrated significantly enhanced degradation performance on semi-crystalline polyethylene terephthalate films under optimized conditions (Cui et al., 2021). Qingbin Li et al. developed a hybrid computational framework integrating machine learning with molecular dynamics simulations to enhance protein thermal stability. The optimal mutant exhibited a T_m increase of 9.3 °C compared with the wild type. Additionally, at 70 °C, the PET degradation rate of this mutant was 46.42-fold higher than that of the wild type (Li et al., 2022). These studies emphasize that molecular modifications effectively improve cutinase thermal stability and further enhance the degradation efficiency of polyester.

In this study, cutinase from *Humicola insolens* was selected for the improvement of its thermostability. Specifically, a combination of strategies was employed to promote the thermostability of HiC. Through iterative combinatorial engineering, an octuple mutant (M8) exhibiting optimized thermal properties was generated. Compared with the wild type, M8 demonstrated a significantly prolonged half-life ($t_{1/2}$), with melting temperature (T_m) and half-inactivation temperature (T) elevated by 13.0 °C and 26.2 °C, respectively. Subsequently, structural analysis and molecular dynamics simulations were performed to elucidate the molecular mechanism of its enhanced performance. Overall, this study demonstrated enhanced thermostability of HiC through synergistic integration of irrational design and computational strategies, while providing mechanistic insights into thermal stabilization. The established methodology offers a valuable framework for engineering other cutinase mutants with improved thermal resilience.

2. Materials and methods

2.1. General

The recombinant plasmid pET20b(+)-hic, previously constructed in our laboratory, served as the base vector for cloning and heterologous expression. *Escherichia coli* (*E. coli*) JM109 (Novagen, Madison, WI, USA) and *E. coli* BL21(DE3) pLysS (TransGen Biotech Co, Ltd, Beijing, China) were used to construct libraries and express proteins, respectively. Bacterial cultures were maintained in LB medium (1 % w/v tryptone, 0.5 % w/v yeast extract, and 1 % w/v NaCl) at 37 °C for genetic manipulation, with protein production conducted in TB medium (2.4 % w/v tryptone, 1.2 % w/v yeast extract, 0.5 % w/v glycerol, 0.231 % w/v KH_2PO_4, and 1.643 % w/v K_2HPO_4) at 25 °C. Restriction endonucleases, alkaline phosphatases, rTaq DNA polymerase, and T4 DNA ligases were sourced from TaKaRa Biotech (Dalian, China), and nucleic acid purification systems (DNA/plasmid/gel extraction kits) were acquired from TianGen Biotech (Beijing, China). The DNA and protein markers, SDS-PAGE gel preparation kits, and loading buffers were supplied by Beyotime Biotechnology (Nantong, China). Polyvinyl acetate (PVAc) and 4-nitrophenyl butyrate (*p*NPB) were purchased from Aladdin (Shanghai, China), while all other analytical-grade chemicals were obtained from

Sinopharm Chemical Reagent (Beijing, China).

2.2. Construction and screening of random mutant libraries

Random mutagenesis of the target gene was carried out via error-prone PCR, utilizing the pET20b(+)-hic plasmid as the template alongside primers MUT-F and MUT-R (see Supplementary materials, Table S1). The amplified PCR product was digested with *Nco* I and *Hind* III for 2 h, purified, and ligated into the pET20b(+) vector pre-treated with the same restriction enzymes and alkaline phosphatase, the ligation mixture was then transformed into *E. coli* BL21 (DE3) pLysS cells. For preliminary screening, the mutant library was evaluated using a 96-deep-well plate cultivation coupled with activity assays.

2.3. PROSS prediction for HiC thermostability

To enhance the stability of the cutinase HiC, the PROSS web tool (Goldenzweig et al., 2016), which integrates evolutionary and energy calculations, was employed to predict mutations that could improve thermal stability. The default settings of PROSS were employed: the crystal structure of cutinase from *Humicola insolens* (PDB ID: 4OYY) with a resolution of 3Å, chain F was used as the template, with a minimum sequence identity of 35 %, a minimum homologous sequence coverage of 75 %, a maximum initial target search number of 4000, and a BLASTp E-value of 1×10^{-4}. Ultimately, the web server provided a total of 9 designs. Selected mutation sites were subsequently validated through site-directed mutagenesis based on experimental requirements.

2.4. Machine learning enhanced the thermostability of HiC

The concept of machine learning was implemented to enhance the thermostability by utilizing an Efficient attention-based Models for Computational Protein Design (EMOCPD), leveraging amino acid microenvironment features to guide the design of HiC (Ling et al., 2024). The model harnessed the integration of language models with image recognition techniques to capture the intricate features of amino acid microenvironments. Subsequently, it underwent finetuning using family-specific information and selected high-probability candidate amino acids to optimize the protein structure. Finally, the effects of mutations were systematically evaluated via folding free energy calculations, providing insights into structural stability and functionality. The model was guided by four progressively interconnected modules: the atomic feature construction module, microenvironment network construction module, deep learning network module, and classifier module.

2.5. Construction, expression, and purification of HiC and mutants

Site-directed mutations were performed using the whole plasmid PCR method, with pET20b(+)-hic as the template. The 2 × Phanta Master Mix (Dye Plus) (Vazyme, Nanjing, China) and mutation primers (see Supplementary materials, Table S1) were used to construct mutations containing single amino acid substitutions. To eliminate the parental template, the PCR products were treated with the methylation-dependent restriction enzyme *Dpn* I. The products were then transformed into *E. coli* JM109 competent cells and screened on LB agar supplemented with ampicillin (100 μg/mL). Positive colonies were isolated for sequence validation through bidirectional Sanger sequencing.

The verified plasmids were subsequently transformed into *E. coli* BL21 (DE3) pLysS competent cells and screened on ampicillin plates (100 μg/mL). Individual colonies were picked and cultured in 10 mL LB medium at 37 °C, 220 rpm for 12 h. To optimize recombinant protein production, 1 % (v/v) pre-culture was transferred to 100 mL TB medium and incubated at 37 °C, 220 rpm for 2–3 h until the cell density (OD_{600}) reached approximately 0.7–0.8. Then, the temperature was adjusted to 25 °C and the fermentation continued for 48 h to induce cutinase expression. Subsequently, the cutinases were purified using a Ni-NTA column and confirmed by sodium dodecyl sulfate–polyacrylamide gel electrophoresis (SDS-PAGE). The target protein was dialyzed against 50 mM Tris-HCl buffer (pH 8.0), and concentrated using a 3000 Da molecular weight cutoff ultrafiltration device. The purified proteins were stored at 4 °C for functional characterization.

2.6. Enzyme activity assay and mutant screening criteria

Cutinase activity was quantified spectrophotometrically using *p*NPB (50 mM) as a substrate in 10 mM Tris-HCl buffer (pH 8.0) at 37 °C, following the protocol established by Chen et al. (Chen et al., 2008). One unit of enzymatic activity corresponds to the liberation of 1 μmol *p*-nitrophenol per minute under standardized assay conditions. During thermostability screening, mutants with soluble expression levels below 60 % of the WT threshold were systematically excluded to ensure functional applicability. Concurrently, mutants retaining no less than 80 % of specific activity were prioritized for subsequent characterization, maintaining a critical balance between stability and catalytic performance. All experiments were performed in triplicate.

2.7. Characterization of cutinase properties

The optimal enzymatic temperature was assessed by measuring hydrolytic activity profiles in 10 mM Tris-HCl buffer (pH 8.0) across a thermal gradient spanning 40–90 °C. Similarly, the optimal pH was evaluated at 37 °C using buffers spanning pH 6.0–10.0. Additionally, for pH stability profiling, purified enzymes were pre-incubated at 37 °C for 24 h in various 100 mM solutions: citrate buffer (pH 3.0–6.0), phosphate buffer (pH 6.0–8.0), Tris-HCl buffer (pH 8.0–9.0) and sodium carbonate buffer (pH 9.0–11.0). The residual hydrolytic activity was then measured and expressed as a percentage of the initial activity.

2.8. Determination of thermodynamic and kinetic stability of cutinase

Thermal stability of cutinases was systematically evaluated through three parameters: the half-life ($t_{1/2}$), the half-inactivation temperature (T), and the melting temperature (T_m) (Chen et al., 2019; Polizzi et al., 2007). To determine $t_{1/2}$ of cutinase, enzyme samples were subjected to time-dependent residual activity measurements following incubation at 60 °C, 65 °C, and 70 °C. The first-order rate constant (k_d) was obtained from the linear regression of ln (residual activity percentage) against incubation time. The equation used was: $\ln A = k_d \times t$ (A: residual activity percentage, t: incubation time), and the half-life values were calculated using: $t_{1/2} = \ln 2/k_d$.

The T values were investigated by measuring the residual activity of the enzymes at different temperatures (ranging from 55 °C to 90 °C) for 1 h. The T values were determined by fitting the residual activity data to a sigmoidal function of temperature, resulting in the thermal inactivation curve.

T_m values were determined by differential scanning calorimetry (DSC) using a nano DSC III system (TA Instruments, New Castle, DE) (Rao et al., 2023). Initially, reference baselines were established with 50 mM Tris-HCl buffer (pH 8.0). Protein samples were diluted to 1.5 mg/mL in the same buffer and analyzed under constant pressure (3 atm) with a temperature ramp from 30 °C to 110 °C at 1 °C/min. Data processing was performed using NanoAnalyze software (TA Instruments), with baseline correction and T_m value calculations based on a two-state transition model.

2.9. Measurements of cutinase kinetic parameters

Enzyme kinetic parameters (k_{cat}, K_m, and k_{cat}/K_m) were resolved using a modified protocol adapted from the methodology established by Wang et al. (2020b). Specifically, hydrolytic activity was quantified under standard reaction conditions (37 °C, 10 mM Tris-HCl buffer pH 8.0) using *p*NPB as a substrate, with substrate concentrations

systematically varied from 5 to 50 mM in 5 mM increments. The maximal reaction velocity (V_{max}) and Michaelis constant (K_m) were derived through nonlinear regression analysis of initial reaction rates using Origin (Origin Lab, USA). The turnover number (k_{cat}) was subsequently determined based on the protein molecular weight and concentration.

2.10. Homology modeling, docking and molecular dynamics (MD) simulations

Homology modeling of cutinase mutants was generated by SWISS-MODEL with the determined HiC crystal structure (PDB ID: 4OYY, 3.0 Å resolution) as the template. Structural alignments and visualization were performed using PyMOL program (https://pymol.org/). MD simulations were performed at 330 K, 340 K, and 350 K to analyze the structural flexibility of the enzyme, with slight methodological modifications adapted from the protocol described by Rao et al. (2022). The docking grid encompassing the catalytic pocket was defined in PyMOL, followed by ligand (*p*NPB) docking into WT and mutant via Ledock software.

The protein structures were solvated in a TIP3P water box and their molecular dynamics were processed using the Amber ff14SB force field (Maier et al., 2015). The proteins were preprocessed to ensure model accuracy, and sufficient sodium and chloride ions were added to the system to achieve charge neutrality. Energy minimization was performed in two stages: the first 5000 steps of steepest descent optimization followed by 5000 steps of conjugate gradient refinement. The system was then gradually heated over 50 ps. This was followed by 200 ps of NPT equilibration to converge the system's pressure and density. Finally, a 100 ns MD simulation was conducted to explore the internal motion trajectories of the molecules. Throughout the simulation, a time step of 2 fs was used, the SHAKE algorithm was used to constrain covalent bonds, while the Langevin thermostat and Berendsen barostat algorithms were employed to control the system's temperature and pressure. All MD simulations were performed using the GPU version of the Amber 18 software package, and trajectory analysis was conducted with AmberTools19 and VMD. Subsequently, trajectory analysis was performed using the cpptraj module to evaluate the root mean square deviation (RMSD), root mean square fluctuation (RMSF), radius of gyration (Rg), solvent accessible surface area (SASA), and hydrogen bonds (H-bonds) of the protein (Roe and Cheatham, 2013). Additionally, the dynamic cross-correlation maps (DCCM) were analyzed using the R package Bio3D (Grant et al., 2006).

2.11. Degradation of PVAc and PET

Based on a modified version of the method described by Yang et al. (2018), the hydrolytic activity of cutinase on adhesives was evaluated using PVAc as a substrate. A 2 % (w/v) solution of PVAc was dissolved in dimethyl sulfoxide, and 1 mL of the substrate solution was mixed with enzyme (10 μg) in a final volume of 10 mL of 50 mM Tris-HCl buffer (pH 8.0), and the reaction was carried out in a water bath shaker at 150 rpm. Subsequently, the liberated acetic acid was quantified via spectrophotometric quantification using a commercial acetic acid assay kit (Megazyme) according to manufacturer specifications. The enzymatic degradation of polyethylene terephthalate (PET) was performed according to the method described by Chen et al. with modifications (Chen et al., 2022). Low-crystallinity PET powder (100 mg) was mixed with 100 μg of enzyme in 100 mM potassium phosphate buffer (pH 8.0) in a total reaction volume of 5 mL for enzymatic depolymerization. The reaction system was incubated at designated temperatures (60 °C, 65 °C, and 70 °C) in a reciprocating water bath (150 rpm). The pH was maintained at 8.0 through periodic addition of 6 M NaOH. Reactions were terminated with 1 mL methanol addition, followed by centrifugation at 8000 rpm for 10 min to collect the supernatant. Hydrolysis products were analyzed via high-performance liquid chromatography (HPLC) using a Athena C18-WP column (4.6 × 250 mm, 5 μm) with a mobile phase of methanol and 1 % (w/v) acetic acid aqueous solution (35:65, v/v) at a flow rate of 0.5 mL/min. Detection was performed at 240 nm, and the column temperature was maintained at 30 °C. Degradation products were identified by comparing retention times with authentic standards and quantified based on the peak area ratio to calibrated standard curves.

2.12. Statistical analysis

Enzymatic activities of WT and mutants were determined through triplicate measurements, with subsequent statistical evaluation conducted using Origin software. All experimental procedures and analytical protocols were executed with a minimum of three biological replicates. Standard deviation calculations and graphical representations were generated through Origin, while statistical significance was assessed via one-way ANOVA and Student's *t*-test (*$P < 0.05$; **$P < 0.01$; ***$P < 0.001$; ****$P < 0.0001$).

3. Results and discussion

3.1. Thermostability enhancement of HiC via random mutagenesis

A high-throughput screening platform was established to improve HiC thermostability through error-prone PCR (epPCR) coupled with 96-well plate-based activity assays. Specifically, to optimize mutagenesis efficiency, three epPCR libraries were generated under varying $MnCl_2$ concentrations (0.1, 0.15, and 0.2 mM), with 0.15 mM identified as optimal based on mutation frequency and library diversity. Approximately 3300 clones (out of ~5000) exhibited esterase activity.

Following primary screening, 90 candidates that demonstrated improved thermal tolerance relative to HiC were advanced to secondary screening (Fig. 1A). Subsequent analysis identified 15 clones displaying enhanced thermal stability, which were further evaluated through shake-flask fermentation analysis. As illustrated in Fig. 1B, the specific activities of the majority of mutants retained over 80 % of WT. Following thermal stability screening, mutants S5 (G8D) and S9 (R51P) were ultimately identified as possessing broad thermal stability while maintaining specific activity, the residual enzyme activities after heat treatment showed 1.28- and 1.34-fold enhancements compared with WT, respectively.

3.2. Thermostability enhancement of HiC via PROSS computational algorithm

The online prediction tool PROSS was utilized to further explore additional potential sites. The output results showed that the online server generated nine potential designs for improved thermostability, with the number of mutations per design ranging from 2 to 34, according to the Rosetta energy score (see Supplementary materials, Table S2). Based on a comprehensive analysis, design 9 was selected for experimental characterization (see Supplementary materials, Table S3). As certain sites had been previously validated, they were excluded from further analysis. Thus, a total of 33 sites underwent mutagenesis, and their expression levels and thermal stability were subsequently assessed.

As illustrated in Fig. 1C, following heat treatment, the results indicated that mutants I36T, A65D, T68D, A130V, R141N, and T164D exhibited improved thermal stability compared with WT, with residual activities increased by 1.36-, 1.52-, 1.67-, 1.63-, 1.41-, and 1.70-fold while maintaining specific activity. Notably, mutants N79A and I178D exhibited marginally reduced specific activities but demonstrated substantial thermal stabilization, retaining 1.69- and 1.40-fold residual activity post-treatment, respectively.

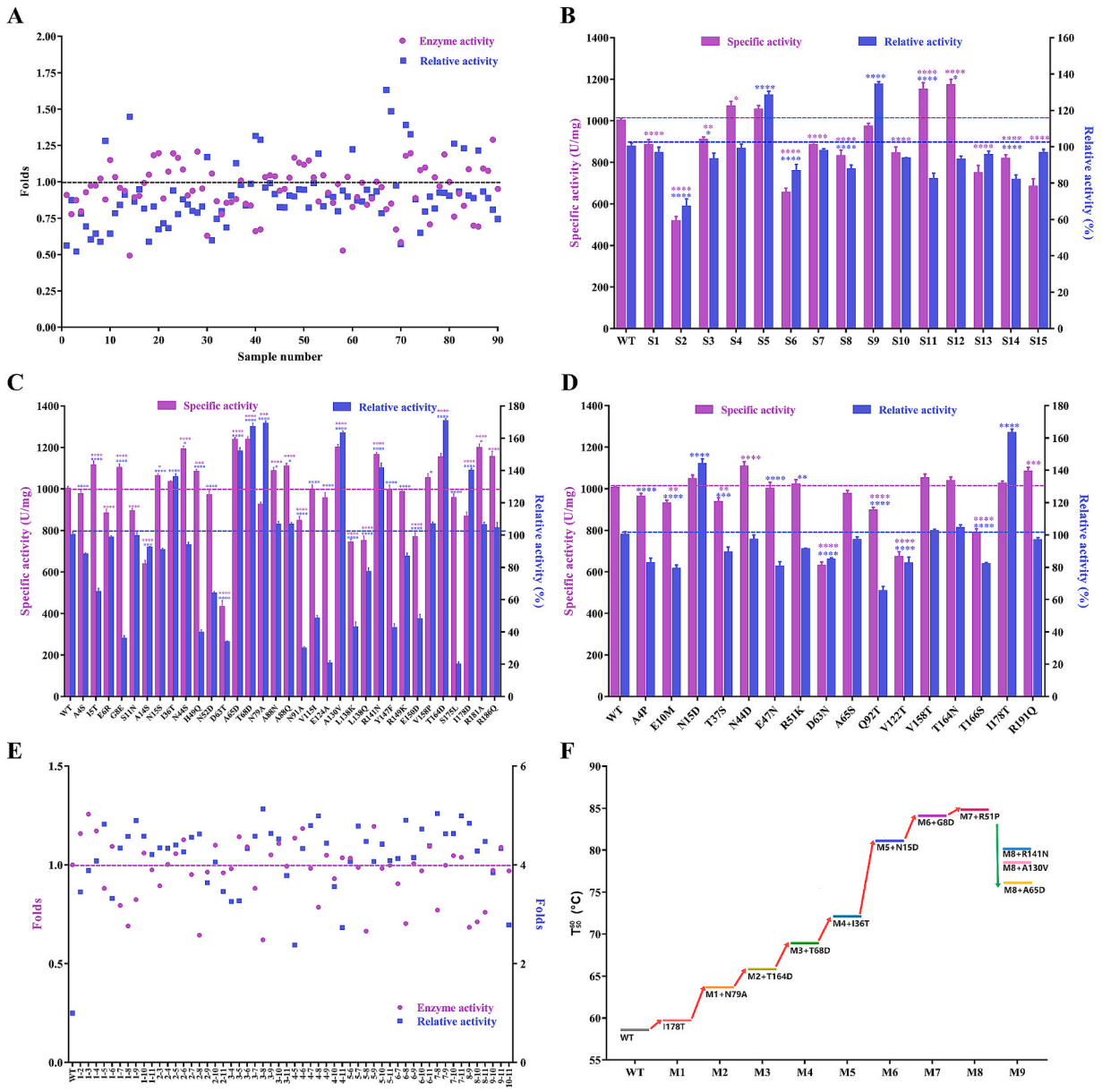

Fig. 1. Thermostability modification of HiC mutants. (A): Primary screening of thermostable mutants. The enzyme activity and relative activity of selected mutants were systematically evaluated, with corresponding data points are shown purple and blue, respectively; (B): Secondary screening of thermostable mutants. Specific activity and relative activity are shown as purple and blue bar graphs, respectively; (C): Thermostability modification of HiC by PROSS designed. Specific activity and relative activity are shown as purple and blue bar graphs, respectively; (D): Thermostability modification of HiC by machine learning. Specific activity and relative activity are shown as purple and blue bar graphs, respectively; (E): Pairwise combinatorial screening of single mutants. Mutants 1–11 correspond to G8D, N15D, I36T, R51P, A65D, T68D, N79A, A130V, R141N, T164D, and I178T, respectively; (F): T values of iterative combinatorial mutants. Only top-performing mutants from each round are shown. The combinatorial strategy involves: I) Pairing the most thermostable mutant from each iteration with all candidates; II) Mutants exhibiting at least 80 % specific activity relative to wild type were prioritized. Enzyme Activity: Enzyme activity is defined as the initial catalytic activity of the mutant relative to WT under standardized assay conditions, prior to heat treatment. Relative Activity: Relative activity is defined as the ratio of residual enzyme activity of the mutant to that of the WT after heat treatment, expressed as a percentage. Specific Activity: Specific activity is defined as the ratio of enzymatic activity to total protein concentration, measured under standardized conditions. Error bars represent the standard deviation from triplicate experiments. * $P < 0.05$; ** $P < 0.01$; *** $P < 0.001$; **** $P < 0.0001$. (For interpretation of the references to colour in this figure legend, the reader is referred to the web version of this article.)

3.3. Thermostability enhancement of HiC via machine learning

The previously described strategies identified multiple mutation sites capable of improving HiC thermostability. In this section, a machine learning framework incorporating four progressively interconnected modules was introduced to predict HiC mutants with enhanced thermal stability. The results indicated that after predicting and optimizing the three-dimensional atomic environment around the amino acids, a total of 16 mutants were identified that met the expectations (see Supplementary materials, Table S4).

As shown in Fig. 1D, the performance of promising mutants identified through machine learning was presented. The results indicated that the specific activities of the majority of mutants exhibited minimal variation when compared with WT. After heat treatment, mutants N15D and I178T displayed improved thermal stability relative to WT and other mutants without compromising specific activity, with residual enzyme activities showing 1.44- and 1.63-fold enhancements compared with WT, respectively. Mutant I178T exhibited a 1.18-fold higher specific

activity and 23 % greater residual activity after thermal treatment compared with I178D (Fig. 1C), demonstrating superior overall performance. Consequently, I178D was excluded from subsequent characterization to focus on mutants with enhanced functional properties.

3.4. Thermostability enhancement of HiC via iterative combinatorial mutagenesis

Previous studies have demonstrated that introducing additional disulfide bonds can significantly increase the protein's melting temperature (Yu et al., 2017), while proline substitution at flexible residues represented another effective strategy for enhancing thermostability (Kun et al., 2014). For instance, the combined engineering of PET2 through homologous modeling, the proline effect and disulfide bond design was successful, ultimately achieving a T_m that was 6.7 °C higher than that of WT (Nakamura et al., 2021). Similarly, structure-guided modification of *Is*PETase using its crystal structure produced a mutant with 8.8 °C higher T_m than the native enzyme (Son et al., 2019). With the advancement of computational strategies, recent developments have enabled targeted stabilization through machine learning and energy-based algorithms (Cui et al., 2021). A hybrid strategy integrating directed evolution and computational protein engineering was implemented to engineer HiC, with intentional exclusion of additional disulfide bonds given the enzyme's inherent structural stabilization by two native disulfide bonds (Cys17-Cys94 and Cys156-Cys163). Excessive disulfide bonds could potentially compromise proper folding and heterologous expression (Nakamura et al., 2021).

Through the three aforementioned strategies, 11 mutation sites enhancing thermal stability were identified, and SDS-PAGE profiles along with T_m values were presented (see Supplementary materials, Figs. S1, S9, and Table S5). Mutants exhibited T_m increases ranging from 0.5 °C to 3.8 °C compared with WT. To investigate the synergistic effects among these beneficial mutations, an iterative combination mutagenesis strategy was employed to accumulate mutation sites. As illustrated in Fig. 1E, the double mutant M2 (I178T/N79A) exhibited the optimal expression levels and residual enzyme activity, with post-heat treatment residual activity increased by 4.99-fold compared with WT. Subsequently, these advantageous mutations were progressively combined to generate the octuple mutant M8 (I178T/N79A/T164D/T68D/I36T/N15D/G8D/R51P). However, mutations A65D, A130V, and R141N failed to exhibit synergistic stabilization effects after nine combinatorial rounds (Fig. 1F). Individually, these mutations likely stabilized distinct regions of the protein to enhance thermal stability (see Supplementary materials, Table S5), their further modifications introduced in the M8 mutant may have disrupted the coordinated conformational dynamics essential for catalysis and substrate binding, generating steric incompatibilities and destabilizing electrostatic interfaces.

3.5. Effects of iterative combinatorial mutagenesis on enzymatic properties

SDS-PAGE analysis of purified HiC and its mutants confirmed homogeneity, with all mutants displaying a single electrophoretic band (see Supplementary materials, Fig. S2). The specific activities of all mutants are presented in Table 1, and the specific activity of M8 reached 1236 U/mg, corresponding to a 1.23-fold enhancement over WT levels, indicating that cumulative point mutations can enhance thermostability without compromising enzymatic function. Subsequently, a comprehensive evaluation of enzymatic properties and thermal tolerance of the iteratively engineered combinatorial mutants was conducted.

The optimal temperatures of engineered mutants were systematically investigated over a range of 40 °C to 90 °C (see Supplementary materials, Fig. S3). The optimal temperature for WT was determined to be 80 °C, and as the mutations were progressively combined, the optimal temperature shifted to higher values. At 90 °C, the residual enzymatic activities of WT and M1 were 52.15 % and 77.83 %, respectively, while the optimal temperatures for remaining mutants increased to 90 °C or higher. This observation suggested that as the accumulation of mutations progresses, the optimal temperature correspondingly rises, a characteristic largely attributed to the enhanced thermal tolerance of mutants.

Additionally, the optimal pH and pH stability of mutants were systematically investigated (see Supplementary materials, Figs. S4 and S5). The results demonstrated that the optimal pH for WT was 8.5, and with the accumulation of mutations, most mutants exhibited improved performance in alkaline conditions compared with the WT. Notably, the optimal pH of M8 shifted to 9.0. Subsequently, the pH stability of mutants was investigated. The cutinase retained over 80 % of its catalytic activity within the pH range of 4.0 to 10.0. However, the stability of WT decreased sharply beyond pH 10.0, with activities of 42.80 % and 17.48 % at pH 10.5 and 11.0, respectively. It was noteworthy that the mutant M8 retained 76.85 % and 68.15 % of its activity at pH 10.5 and 11.0, representing 34.05 % and 50.67 % improvements over WT levels, respectively. Overall, these results demonstrate that combinatorial

Table 1
Thermal stability parameters and kinetic parameters of WT and its iterative mutants.

Name	Mutants	$t_{1/2}$ (min, 60 °C)	$t_{1/2}$ (min, 65 °C)	$t_{1/2}$ (min, 70 °C)	T (°C)	△T (°C)	T_m (°C)	△T_m (°C)	Specific activity of the purified Cutinase (U/mg)	K_m (mM)	k_{cat} (s^{-1})	k_{cat}/K_m (s^{-1} mM^{-1})	V_{max} (U/mg)
WT	/	6.8	1.1	0.6	58.6	0	62.1	0	1003 ± 32.5	0.21	0.31	1.43	905.7 ± 52
M1	I178T	53.1	1.6	0.8	59.7	1.1	63.3	1.2	1015 ± 29.8	0.23	0.33	1.43	984.9 ± 57
M2	I178T/N79A	7011.6	21.7	1.2	63.7	5.1	67.7	5.6	857 ± 39.3	0.27	0.29	1.08	871.5 ± 69
M3	I178T/N79A/T164D	12022.2	167.7	2.1	65.8	7.2	68.6	6.5	925 ± 35.6	0.23	0.29	1.29	870.2 ± 47
M4	I178T/N79A/T164D/T68D	23673.6	3146.4	34.9	68.9	10.3	71.4	9.3	1049 ± 39.4	0.21	0.37	1.72	1091 ± 75
M5	I178T/N79A/T164D/T68D/I36T	/	5299.8	173.9	72.1	13.5	72.4	10.3	1084 ± 27.5	0.12	0.36	2.96	1075 ± 40
M6	I178T/N79A/T164D/T68D/I36T/N15D	/	6709.2	531.0	81.1	22.5	73.1	11.0	1063 ± 28.1	0.11	0.4	3.65	1185 ± 41
M7	I178T/N79A/T164D/T68D/I36T/N15D/G8D	/	7195.8	1884.6	84.1	25.5	74.3	12.2	1152 ± 27.2	0.12	0.38	3.09	1117 ± 39
M8	I178T/N79A/T164D/T68D/I36T/N15D/G8D/R51P	/	8921.4	2389.2	84.8	26.2	75.1	13.0	1236 ± 35.7	0.12	0.43	3.48	1273 ± 42

mutagenesis significantly enhances alkaline resilience, expanding the functional range of HiC under industrially relevant alkaline conditions.

3.6. Thermal stability characterization of mutants

The ability of the enzyme to retain its activity despite undergoing irreversible denaturation is referred to as kinetic stability (Polizzi et al., 2007). Specifically, the thermal kinetic stability parameters were measured at different temperatures of WT and its mutants (Table 1 and see Supplementary materials, Figs. S6–S8). Notably, at 65 °C, the $t_{1/2}$ values of WT and M8 were 1.1 min and 8921.4 min, respectively, with the half-life of M8 extended by 8110-fold compared with the WT. Moreover, at 70 °C, the half-life of WT was merely 0.6 min, whereas the $t_{1/2}$ of mutant M8 was 2389.2 min, signifying a remarkable 3982-fold enhancement compared with WT. Meanwhile, the T value was determined by incubating samples at various temperatures (55–90 °C) for 60 min and measuring the residual activity. The T values of WT and engineered mutants are summarized in Table 1 and Fig. 1F. The results indicated that the T value for WT was 58.6 °C, while mutant M8 demonstrated a 26.2 °C improvement, achieving a T value of 84.8 °C.

In contrast to kinetic stability, thermodynamic stability pertains to the equilibrium unfolding behavior of the protein conformation (Polizzi et al., 2007). The T_m values of WT and mutant enzymes were determined via DSC, with results summarized (Table 1 and see Supplementary materials, Fig. S9). DSC analysis revealed the T_m value of 62.1 °C for WT, and mutants M1-M8 exhibited significantly elevated melting temperatures ranging from 63.3 °C to 75.1 °C, which were 1.2–13.0 °C higher than the WT value. In summary, the comprehensive characterization revealed that M8 not only maintained optimal catalytic efficiency but also demonstrated significantly enhanced thermal stability compared with WT, achieving simultaneous optimization of enzymatic performance and heat resistance.

3.7. Kinetic parameters of mutants

The kinetic parameters of WT and mutant enzymes were determined using *p*NPB as a substrate at pH 8.0 and 37 °C. The results in Table 1 showed that the K_m of M8 was 42.5 % lower compared with WT, indicating an enhanced affinity for the substrate in M8. The turnover rate, k_{cat}, increased by 40.6 %, representing an increase in the ability of M8 to transform substrates. Additionally, the k_{cat}/K_m value of M8 surpassed WT levels by 44.5 %, demonstrating synergistic optimization of both

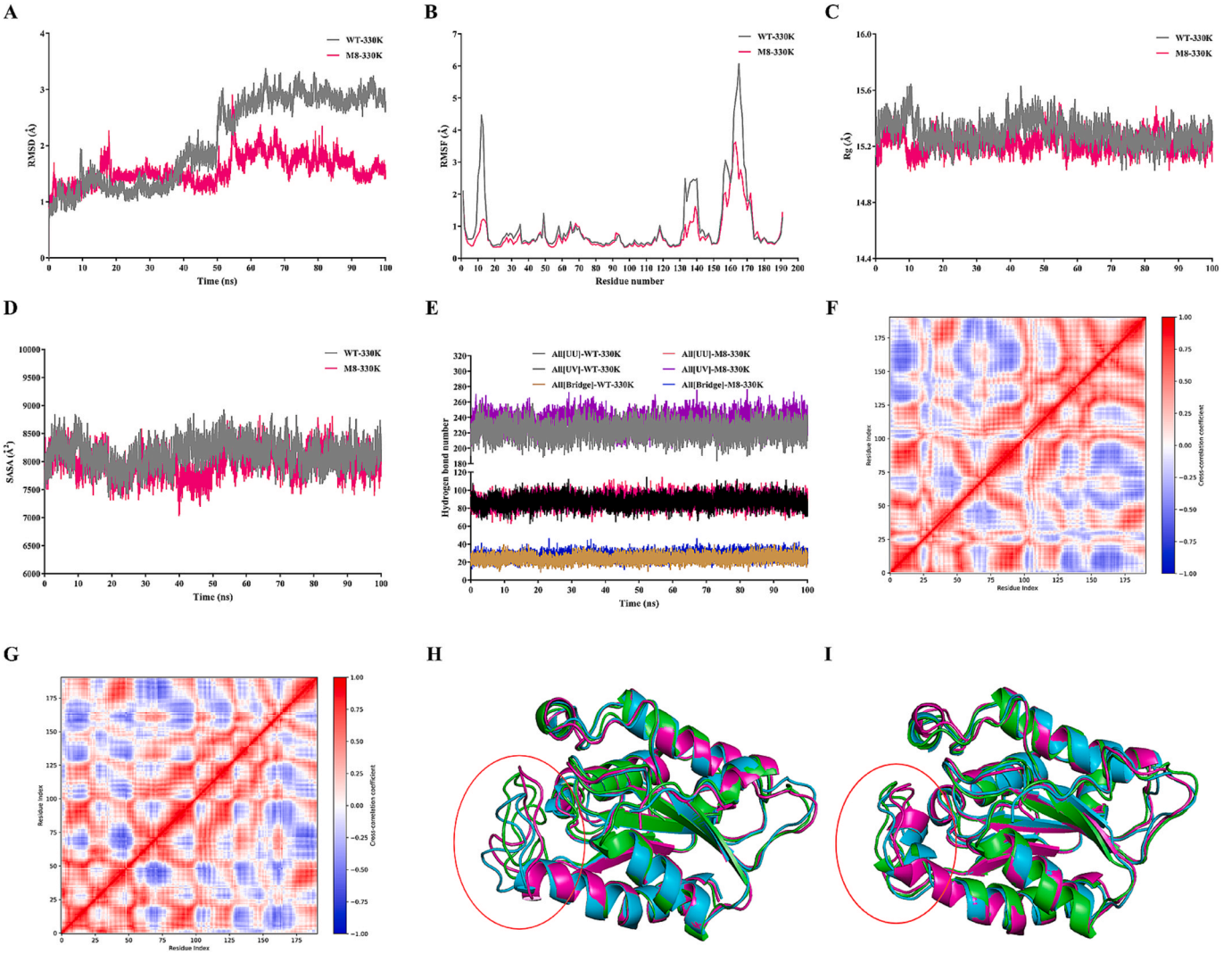

Fig. 2. Molecular dynamics simulations elucidated the thermal stability of WT and M8. (A): Root mean square deviation (RMSD); (B): Root mean square fluctuation (RMSF); (C): Radius of gyration Analysis (Rg); (D): Solvent accessible surface areas (SASA); (E): The number of hydrogen bonds (H-bonds); (F): DCCM analysis of WT; (G): DCCM analysis of M8; (H): Structural changes of WT in 0–100 ns; (I): Structural changes of M8 in 0–100 ns. The structural snapshots at 0, 50, and 100 ns are displayed as green, blue, and magenta ribbons, respectively. (For interpretation of the references to colour in this figure legend, the reader is referred to the web version of this article.)

substrate recognition and catalytic throughput. Following 100 ns MD simulations at 310 K (see Supplementary materials, Fig. S10), comparative analysis of distance distributions between Ser105 hydroxyl oxygen and *p*NPB carbonyl carbon revealed WT deviations beyond catalytic thresholds after 10 ns, prompting a focus on initial 10 ns trajectories. Structural engineering through mutagenesis reduced the average nucleophilic attack distance during the initial 10 ns phase from 5.32 Å in WT to 3.93 Å in M8, maintaining proximity conducive to efficient catalysis. Overall, these results collectively demonstrate that combinatorial mutagenesis not only enhances substrate affinity but also improves overall enzymatic efficiency.

3.8. Molecular dynamics simulations elucidate mechanisms of thermal stability

To elucidate the impact of mutations on the structural stability of cutinase, MD simulations of WT and M8 at 330 K-350 K (Fig. 2 and see Supplementary materials, Figs. S11 and S12) for a duration of 100 ns were performed, and then their trajectories were analyzed. As shown in Fig. 2A, the RMSD analysis revealed that M8 maintained consistently lower structural fluctuations than WT, indicating an increased structural rigidity and enhanced thermal stability of M8 mutant, underscoring the beneficial impact of the mutations on the protein's overall stability. The RMSF results in Fig. 2B revealed that the native structure flexibility was considerably higher than that of M8, which includes the regions of 5–15, 25–35, 50–60, 130–140, and 155–170. It was noteworthy that the most significant reductions were observed in the 130–140 and 155–170 residue regions, which included the catalytic triad of cutinase. The results shown in Fig. 2C indicated that the Rg of WT was consistently higher than that of M8 during the simulation of 100 ns. The average Rg values of WT and M8 were 15.30 Å and 15.22 Å, respectively. Fig. 2D presents the SASA values of WT and M8 at 330 K. During the 100 ns simulation, the average SASA values for WT and M8 were 8136 $Å^2$ and 7976 $Å^2$, respectively, demonstrating enhanced structural compaction through combinatorial mutagenesis.

As the MD simulation temperature increased to 340 K and 350 K (see Supplementary materials, Figs. S11 and S12), apart from the RMSF change, RMSD, Rg and SASA basically reflected the trends observed at 330 K. Notably, M8 demonstrated markedly reduced RMSF deviations in the 130–150 residue region compared with WT, despite temperature-dependent conformational fluctuations. These findings demonstrate that M8 throughout the simulation underscores its more compact structural arrangement at elevated temperatures, which contributes to its enhanced ability to withstand higher temperatures while maintaining functional integrity (Pouyan et al., 2022; Wang et al., 2020a). In summary, this increased structural compactness and stability make M8 more resilient to thermal denaturation compared with WT.

Additionally, to further evaluate the stability of WT and M8 during the MD process, the number of hydrogen bonds within their protein structures was counted. Fig. 2E illustrates the temporal evolution of solute–solute and solute–solvent hydrogen bonds, as well as solute–solvent-solute bridging interactions. The results indicated that there was negligible disparity in the number of solute–solute hydrogen bonds between WT and M8, with both fluctuating around 88. However, the mutant M8 exhibited a higher number of solute–solvent hydrogen bonds and solute–solvent-solute bridging interactions compared with WT. The average number of solute–solvent hydrogen bonds for WT and M8 was 222.8 and 234.9, while the average solute–solvent-solute bridging interactions was 24.1 and 27.1, respectively. Similar trends in hydrogen bonds variations were observed across varying thermal conditions during molecular dynamics simulations (see Supplementary materials, Figs. S11 and S12). These findings demonstrate that enhanced hydrogen bonding networks in the mutant reinforce structural integrity through improved hydration dynamics and interfacial water coordination, thereby increasing thermal resilience under elevated temperature conditions.

Dynamic cross-correlation map (DCCM) provides critical insights into protein conformational dynamics by quantifying time-dependent residue correlations during molecular simulations. This analytical approach identifies rigid and flexible structural domains through correlated motion patterns, elucidating mechanistic relationships between global dynamics and functional stability (Qiu et al., 2024). An analysis of the residue correlation networks of the MD trajectories as illustrated in Fig. 2F and G, analysis suggested that combinatorial mutations had induced significant changes in residue correlations, with some transitions from positive to negative correlations or a general weakening of correlations. This shift indicated an enhanced independence in internal dynamics, potentially contributing to improved thermal stability.

Subsequently, the conformational dynamics of key structural regions was investigated through molecular dynamics trajectory analysis. As illustrated in Fig. 2H and I, the structural snapshots at 0, 50, and 100 ns were extracted from MD trajectories and visualized as green, blue, and magenta ribbons, respectively. The results indicated that at the 50 ns mark, the protein structure of WT exhibited pronounced conformational drift from its initial conformation, while mutant M8 maintained near-native geometry. As time progressed to 100 ns, the WT exhibited more significant structural deviation, whereas mutant M8 displayed structural integrity with minimal conformational fluctuations. Comparative spatiotemporal analysis of structural displacements demonstrated predominant conformational reorganization within the catalytic triad and adjacent loop regions.

3.9. Structural analysis reveals mechanisms of thermal stability

The SWISS-MODEL was employed to construct a model of M8 mutant, which was subsequently compared with HiC using PyMOL. It is generally accepted that when the root mean square deviation (RMSD) between structures is within 2 Å, the structural similarity is considered high (Zhang et al., 2024). Fig. 3A illustrates the structural superposition, with green and blue ribbons representing the WT and M8, respectively. The maximum RMSD difference was 0.057 Å, with 181 amino acids aligned at the same level, indicating that the protein structure of M8 did not undergo significant changes compared with WT.

To further investigate the alterations in intramolecular interactions before and after the mutation, the residue interaction networks were evaluated using the Ring4.0 online server (Del Conte et al., 2024). Comparative analysis revealed that M8 mutant exhibited two additional intramolecular hydrogen bonds and 15 enhanced van der Waals interactions compared with WT (Fig. 3B–C and see Supplementary materials, Table S6), likely contributing to its improved thermal resilience. As shown in Fig. 3D–E, site-specific analysis of intramolecular interactions revealed enhanced hydrogen bonding and van der Waals contacts at mutation sites G8D, N15D, R51P, and T164D, with distinct interaction networks remodeling observed at each modified residue. In summary, the enhanced catalytic performance and thermal stability of M8 likely emerged from localized restructuring of molecular interaction networks, driven by subtle global conformational rearrangements that optimized both structural rigidity and functional plasticity.

Enhanced thermostability and catalytic performance were achieved through rational engineering of surface charge distribution by strategically substituting charged and neutral amino acid residues (Li et al., 2023; Zhao et al., 2020). As illustrated in Fig. 4A and B, electrostatic potential analysis of cutinase revealed significant charge redistribution at positions 8, 15, 68 and 164, with mutant M8 displaying enhanced negative surface charge density compared with WT. The mutations at these four amino acid regions in mutant M8 could perturb local charge distributions, modifying the surface microenvironment and potentially influencing active-site pKa values, ultimately enhancing the thermal stability of cutinase. The isoelectric point (pI) was computationally determined using the ProtParam tool on the ExPASy server, showing a decrease from 8.43 for WT to 5.40 for M8, thereby validating the

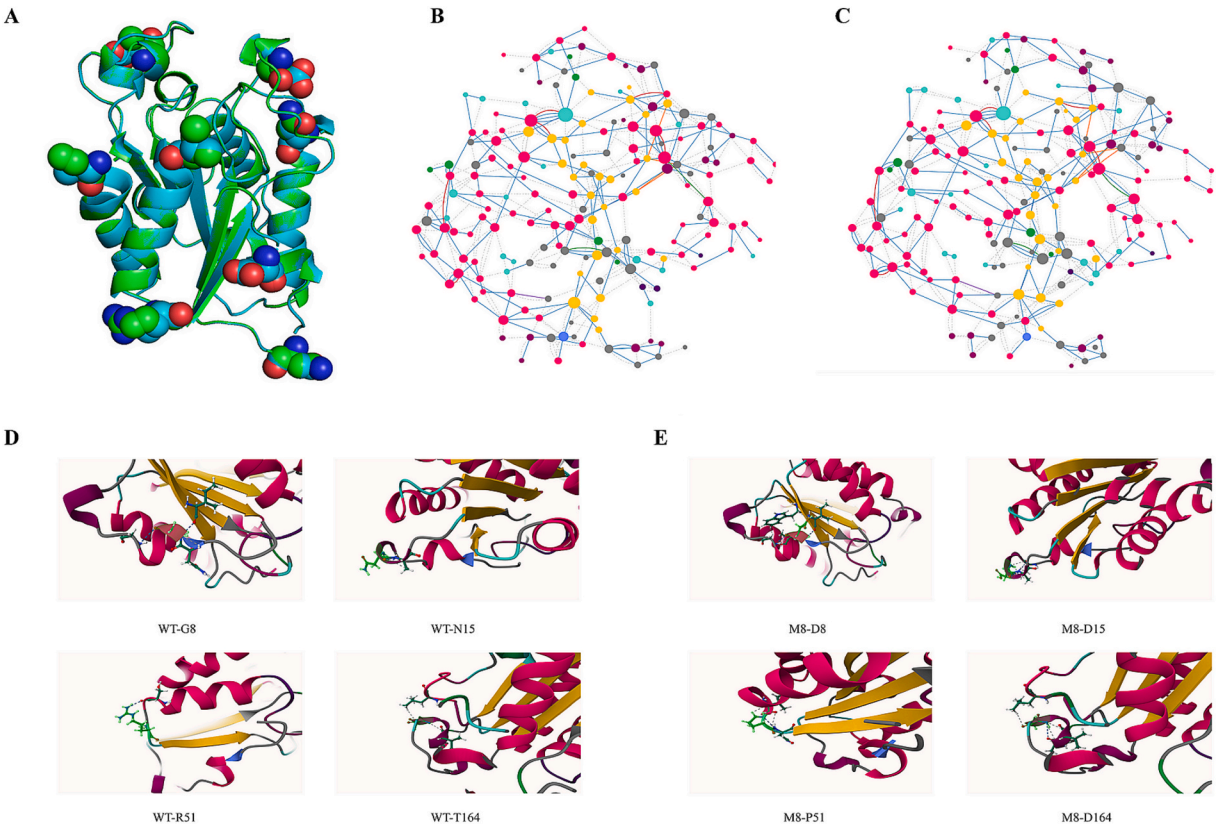

Fig. 3. Comparative analysis of structural discrepancies between WT and M8. (A): Comparative structural analysis of WT and M8; (B): Residue interaction network of WT; (C): Residue interaction network of M8; (D): Assessment of hydrogen bonding and van der Waals interactions in WT; (E): Assessment of hydrogen bonding and van der Waals interactions in M8.

electrostatic redistribution hypothesis. Furthermore, hydrophilic surface interactions and hydrophobic core packing were considered critical factors for enhancing protein thermal stability (Kamal et al., 2011; Zeng et al., 2022). Hydrophobicity analysis was conducted and the results are shown in Fig. 4C and D. Specifically, the hydrophobicity slightly increased in the regions of sites 15 and 51, while the other sites were reduced to varying degrees. In WT, sites 36, 68, and 164 exhibited strong hydrophobicity, while sites 15 and 51 demonstrated pronounced hydrophilicity. Hydrophobic analysis revealed optimized surface hydrophobicity patterns in the mutant. The enhanced thermostability of M8 likely originated from strategic surface residue engineering involving balanced integration of hydrophilic and hydrophobic groups, which improved aqueous solubility. This modification promoted hydration shell stabilization and surface charge repulsion, effectively reducing thermal aggregation while preserving structural integrity.

3.10. PVAC and PET hydrolysis

Polyvinyl acetate, a pressure-sensitive adhesive prevalent in paper manufacturing, constitutes a major source of stickies deposition challenges (Hong et al., 2019). Cutinase can hydrolyze the ester bonds in PVAc, generating acetic acid and polyvinyl alcohol to diminish adhesive properties. Under typical conditions, the temperature of wastepaper pulp is maintained around 60 °C, however, equipment aging or environmental factors may elevate temperatures beyond this threshold (Zhang et al., 2016). Therefore, the degradation capability of cutinase on PVAc at elevated thermal conditions was investigated. As illustrated in Fig. 5A, the hydrolytic efficiency of WT and M8 on PVAc was assessed at various temperatures. The results indicated that at 50 °C and 55 °C, both mutants exhibited equivalent degradation capacity. However, at elevated temperatures, the WT exhibited significantly reduced catalytic efficiency, producing only half the amount of acetic acid compared with M8 at 60 °C. The WT demonstrated a rapid decline in PVAc hydrolytic capacity when exposed to temperatures exceeding 60 °C, whereas the engineered mutant retained full catalytic functionality under identical thermal stress conditions. The observed drop in activity above 60 °C likely reflects partial unfolding of the enzyme, as supported by MD simulations showing reduced binding pocket stability at temperatures approaching T_m (Fig. 2 and see Supplementary materials, Figs. S11 and S12). The expanded thermal optimum directly addressed a critical limitation in industrial enzyme applications by demonstrating sustained superior catalytic efficiency of the M8 mutant under elevated thermal stress conditions.

The PET hydrolytic performance of WT and M8 mutant was evaluated at 60 °C, 65 °C, and 70 °C (Fig. 5B and see Supplementary materials, Fig. S13). The results revealed a notable decline in the degradation efficiency of both WT and M8 at 65 °C and 70 °C, which may be attributed to the enhanced crystallinity of PET hindering enzyme-substrate binding. Previous studies have demonstrated that the crystallinity of PET increases with elevated temperatures and prolonged incubation time (Tournier et al., 2020). The M8 mutant demonstrated significantly enhanced depolymerization efficiency at 60 °C compared with WT. After 48h incubation, M8 achieved TPA and MHET yields of 41.5 mg/mL (249.7 μM) and 14.3 mg/mL (68.1 μM), respectively, corresponding to 1.56-fold and 2.46-fold improvements relative to WT performance under identical reaction conditions. Notably, while the WT showed negligible product accumulation beyond 48 h, the M8 mutant maintained a gradual increase in TPA release over time, further confirming its enhanced depolymerization efficiency under moderate thermal conditions. Moreover, bis(hydroxyethyl) terephthalate (BHET) was not observed in the reaction products, indicating rapid enzymatic conversion of intermediate oligomers to TPA and MHET. This absence of BHET

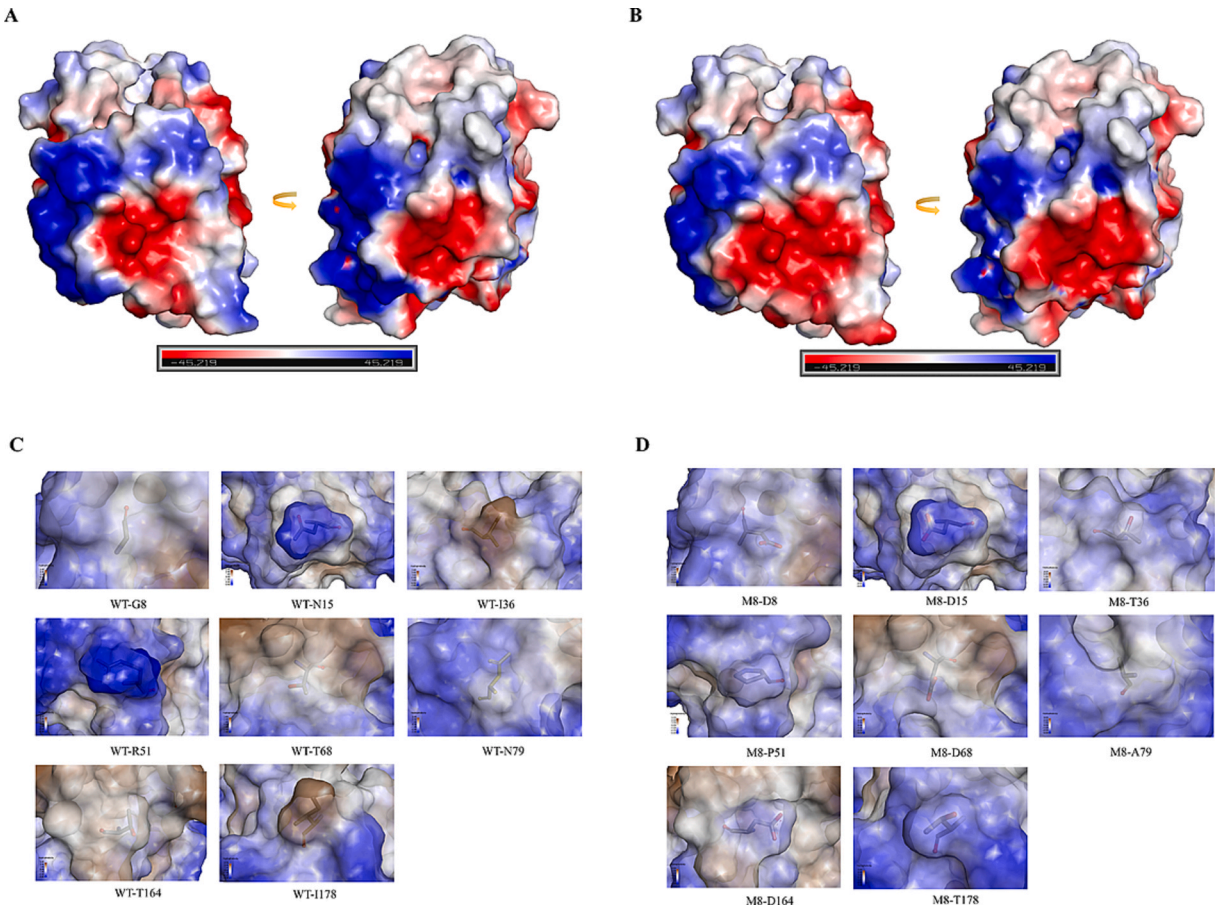

Fig. 4. Overall surface charge distribution and hydrophobicity analysis of WT and M8. (A): Electrostatic potential analysis of WT; (B): Electrostatic potential analysis of M8. Blue and red represent positive and negative charges, respectively; (C): Hydrophobicity analysis of WT; (D): Hydrophobicity analysis of M8. Brown and blue represent the hydrophobicity and hydrophilicity of the regions, respectively. (For interpretation of the references to colour in this figure legend, the reader is referred to the web version of this article.)

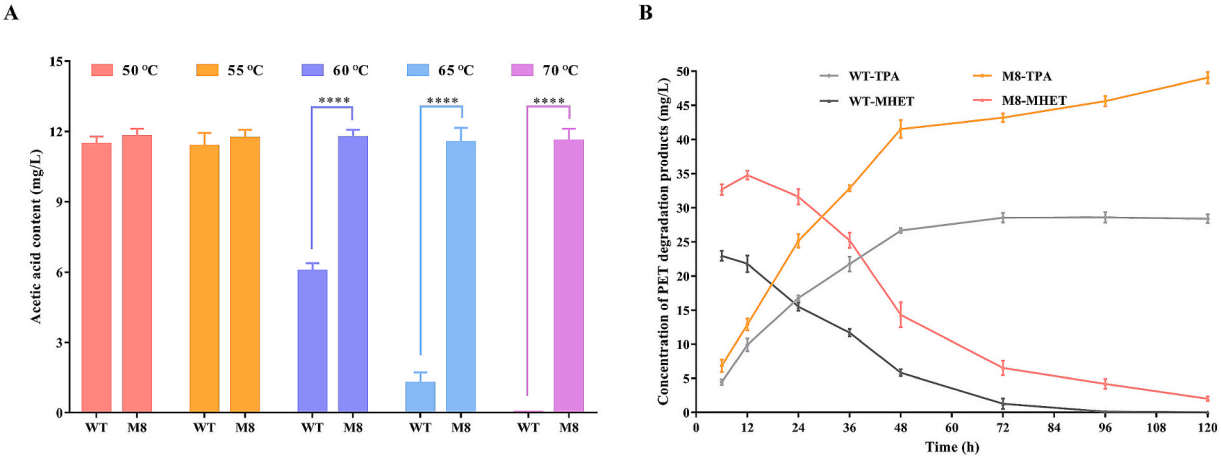

Fig. 5. Analysis of hydrolysis performance of WT and M8. (A): The hydrolytic efficiency toward PVAC under varying temperature conditions; (B): The PET hydrolytic performance was evaluated at 60 °C. Error bars represent the standard deviation from triplicate experiments. * $P < 0.05$; ** $P < 0.01$; *** $P < 0.001$; **** $P < 0.0001$.

accumulation is advantageous for industrial processes, as it minimizes downstream purification steps and enhances overall process efficiency.

Although M8 demonstrated improved catalytic efficiency for the small-molecule substrate *p*NPB (Table 1), its activity on polymeric substrates such as PVAc and PET remained similar to that of the wild-type enzyme (Fig. 5), likely due to spatial limitations caused by the narrow active site of HiC. Future efforts will prioritize redesigning substrate-accessibility features, including loop extensions and adjustments to surface hydrophobicity, to enhance compatibility between small-molecule catalytic efficiency and enzymatic processing of polymeric substrates.

4. Conclusion

This investigation established an integrated protein engineering framework combining error-prone PCR, computationally-assisted design strategies, and machine learning to enhance the thermal stability of cutinase derived from *Humicola insolens*. An octuple mutant was identified through iterative combinatorial screening, demonstrating optimized $t_{1/2}$, T_m, and T values. Additionally, the catalytic parameters and alkali resistance of mutant M8 were significantly enhanced. MD simulations and structural analyses revealed that localized bond network reorganization, coupled with optimized surface residue hydrophobicity and electrostatic complementarity, directly enhance structural rigidity through global conformational optimization, thereby improving cutinase thermostability. In summary, the methodological framework developed here provides a blueprint for overcoming thermal limitations in industrial enzymes, particularly for applications requiring operational stability under extreme process conditions.

CRediT authorship contribution statement

Shiheng Chen: Conceptualization, Investigation, Data curation, Formal analysis, Writing – original draft, Writing – review & editing, Software, Methodology. **Lei Wang:** Writing – original draft, Validation, Investigation, Data curation. **Demin Kong:** Writing – original draft, Software, Methodology. **Zhisheng Wei:** Validation, Investigation, Data curation. **Xiaoqi Ling:** Data curation. **Zhaohong Deng:** Data curation. **Fengshan Zhang:** Funding acquisition. **Lingqia Su:** Writing – review & editing. **Zhanzhi Liu:** Funding acquisition. **Jing Wu:** Project administration, Methodology, Funding acquisition, Conceptualization. **Sheng Chen:** Writing – review & editing, Supervision, Resources, Project administration, Funding acquisition.

Declaration of competing interest

The authors declare that they have no known competing financial interests or personal relationships that could have appeared to influence the work reported in this paper.

Acknowledgement

This work was supported by the National Key Research and Development Program of China (No. 2019YFA0706900), the Taishan Industrial Experts Program (No. tscx202306145), the Yellow River Delta Industrial Leading Talent Program (No. DYRC20200205), the China Postdoctoral Science Foundation (No. 2023M731167), the Jiangsu Province Key Research and Development Program (No. BE2021625).

Appendix A. Supplementary data

Supplementary data to this article can be found online at https://doi.org/10.1016/j.biortech.2025.132882.

Data availability

Data will be made available on request.

References

Chen, C., Su, L., Xu, F., Xia, Y., Wu, J., 2019. Improved thermostability of maltooligosyltrehalose synthase from arthrobacter ramosus by directed evolution and site-directed mutagenesis. J. Agric. Food Chem. 67 (19), 5587–5595.
Chen, J., Wang, Q., Hua, Z., Du, G., 2007. Research and application of biotechnology in textile industries in China. Enzyme Microb. Technol. 40 (7), 1651–1655.
Chen, S., Su, L., Chen, J., Wu, J., 2013. Cutinase: characteristics, preparation, and application. Biotechnol. Adv. 31 (8), 1754–1767.
Chen, S., Tong, X., Woodard, R.W., Du, G., Wu, J., Chen, J., 2008. Identification and characterization of bacterial cutinase. J. Biol. Chem. 283 (38), 25854–25862.
Chen, X.-Q., Guo, Z.-Y., Wang, L., Yan, Z.-F., Jin, C.-X., Huang, Q.-S., Kong, D.-M., Rao, D.-M., Wu, J., 2022. Directional-path modification strategy enhances PET hydrolase catalysis of plastic degradation. J. Hazard. Mater. 433, 128816.
Cui, Y., Chen, Y., Liu, X., Dong, S., Tian, Y.e., Qiao, Y., Mitra, R., Han, J., Li, C., Han, X., Liu, W., Chen, Q., Wei, W., Wang, X., Du, W., Tang, S., Xiang, H., Liu, H., Liang, Y., Houk, K.N., Wu, B., 2021. Computational redesign of a PETase for plastic biodegradation under ambient condition by the GRAPE strategy. ACS Catal. 11 (3), 1340–1350.
Del Conte, A., Camagni, G.F., Clementel, D., Minervini, G., Monzon, A.M., Ferrari, C., Piovesan, D., Tosatto, S.C.E., 2024. RING 4.0: faster residue interaction networks with novel interaction types across over 35,000 different chemical structures. Nucl. Acids Res. 52 (W1), W306–W312.
Dutta, K., Sen, S., Veeranki, V.D., 2009. Production, characterization and applications of microbial cutinases. Process. Biochem. 44 (2), 127–134.
Goldenzweig, A., Goldsmith, M., Hill, S.E., Gertman, O., Laurino, P., Ashani, Y., Dym, O., Unger, T., Albeck, S., Prilusky, J., Lieberman, R.L., Aharoni, A., Silman, I., Sussman, J.L., Tawfik, D.S., Fleishman, S.J., 2016. Automated structure- and sequence-based design of proteins for high bacterial expression and stability. Mol. Cell 63 (2), 337–346.
Grant, B.J., Rodrigues, A.P.C., ElSawy, K.M., McCammon, J.A., Caves, L.S.D., 2006. Bio3d: an R package for the comparative analysis of protein structures. Bioinformatics 22 (21), 2695–2696.
Hong, R., Su, L., Chen, S., Long, Z., Wu, J., 2017. Comparison of cutinases in enzymic deinking of old newsprint. Cellul. 24 (11), 5089–5099.
Hong, R., Su, L., Wu, J., 2019. Cutinases catalyze polyacrylate hydrolysis and prevent their aggregation. Polym. Degrad. Stab. 159, 23–30.
Jones, J.B., Enoch, K.C.N., Christine, L., Kazlauskas, R.J., 2020. Consensus Finder web tool to predict stabilizing substitutions in proteins. Methods Enzymol. 643, 129–148.
Kamal, M.Z., Ahmad, S., Molugu, T.R., Vijayalakshmi, A., Deshmukh, M.V., Sankaranarayanan, R., Rao, N.M., 2011. In vitro evolved non-aggregating and thermostable lipase: structural and thermodynamic investigation. J. Mol. Biol. 413 (3), 726–741.
Kun, W., Huiying, L., Jian, T., Ossi, T., Huoqing, H., Pengjun, S., Huifang, H., Caihong, W., Shuanghe, W., Bin, Y., 2014. Thermostability improvement of a streptomyces xylanase by introducing proline and glutamic acid residues. Appl. Environ. Microbiol. 80 (7), 2158–2165.
Li, Q., Zheng, Y., Su, T., Wang, Q., Liang, Q., Zhang, Z., Qi, Q., Tian, J., 2022. Computational design of a cutinase for plastic biodegradation by mining molecular dynamics simulations trajectories. Comput. Struct. Biotechnol. J. 20, 459–470.
Li, Y., Tang, X., Chen, L., Ma, A., Zhu, W., Huang, W., Li, J., 2023. Improvement of the fibrinolytic activity, acid resistance and thermostability of nattokinase by surface charge engineering. Int. J. Biol. Macromol. 253, 127373.
Ling, X., Cai, C., Deng, Z., Wang, L., Wei, Z., Wu, J., 2024. EMOCPD: Efficient Attention-based Models for Computational Protein Design Using Amino Acid Microenvironment.
Liu, K., Zhao, G., He, B., Chen, L., Huang, L., 2012. Immobilization of pectinase and lipase on macroporous resin coated with chitosan for treatment of whitewater from papermaking. Bioresour. Technol. 123, 616–619.
Liu, Y., Kuhlman, B., 2006. RosettaDesign server for protein design. Nucl. Acids Res. 34 (Web Server), W235–W238.
Maier, J.A., Martinez, C., Kasavajhala, K., Wickstrom, L., Hauser, K.E., Simmerling, C., 2015. ff14SB: improving the accuracy of protein side chain and backbone parameters from ff99SB. J. Chem. Theory Comput. 11 (8), 3696–3713.
Musil, M., Stourac, J., Bendl, J., Brezovsky, J., Prokop, Z., Zendulka, J., Martinek, T., Bednar, D., Damborsky, J., 2017. FireProt: web server for automated design of thermostable proteins. Nucl. Acids Res. 45 (W1), W393–W399.
Nakamura, A., Kobayashi, N., Koga, N., Iino, R., 2021. Positive charge introduction on the surface of thermostabilized PET hydrolase facilitates PET binding and degradation. ACS Catal. 11 (14), 8550–8564.
Oda, M., Yamagami, Y., Inaba, S., Oida, T., Yamamoto, M., Kitajima, S., Kawai, F., 2018. Enzymatic hydrolysis of PET: functional roles of three Ca2+ ions bound to a cutinase-like enzyme, Cut190*, and its engineering for improved activity. Appl. Microbiol. Biotechnol. 102 (23), 10067–10077.
Polizzi, K.M., Bommarius, A.S., Broering, J.M., Chaparro-Riggers, J.F., 2007. Stability of biocatalysts. Curr. Opin. Chem. Biol. 11 (2), 220–225.
Pouyan, S., Lagzian, M., Sangtarash, M.H., 2022. Enhancing thermostabilization of a newly discovered α-amylase from Bacillus cereus GL96 by combining computer-aided directed evolution and site-directed mutagenesis. Int. J. Biol. Macromol. 197, 12–22.
Qiu, S., Ju, C.-L., Wang, T., Chen, J., Cui, Y.-T., Wang, L.-Q., Fan, F.-F., Huang, J., 2024. Evolving ω-amine transaminase *At*ATA guided by substrate-enzyme binding free energy for enhancing activity and stability against non-natural substrates. Appl. Environ. Microbiol. 90 (7), e00543–e00624.
Rao, D., Huo, R., Yan, Z., Guo, Z., Liu, W., Lu, M., Luo, H., Tao, X., Yang, W., Su, L., Chen, S., Wang, L., Wu, J., 2023. Multiple approaches of loop region modification for thermostability improvement of 4,6-α-glucanotransferase from Limosilactobacillus fermentum NCC 3057. Int. J. Biol. Macromol. 233, 123536.
Rao, D., Wang, L., Huo, R., Su, L., Guo, Z., Yang, W., Wei, B., Tao, X., Chen, S., Wu, J., 2022. Trehalose promotes high-level heterologous expression of 4,6-α-glucanotransferase GtfR2 in Escherichia coli and mechanistic analysis. Int. J. Biol. Macromol. 210, 315–323.
Reetz, M.T., Carballeira, J.D., 2007. Iterative saturation mutagenesis (ISM) for rapid directed evolution of functional enzymes. Nat. Protoc. 2 (4), 891–903.
Roe, D.R., Cheatham, T.E., 2013. PTRAJ and CPPTRAJ: software for processing and analysis of molecular dynamics trajectory data. J. Chem. Theory Comput. 9 (7), 3084–3095.

Son, H.F., Cho, I.J., Joo, S., Seo, H., Sagong, H.-Y., Choi, S.Y., Lee, S.Y., Kim, K.-J., 2019. Rational Protein Engineering of Thermo-Stable PETase from Ideonella sakaiensis for Highly Efficient PET Degradation. ACS Catal. 9 (4), 3519–3526.

Tournier, V., Topham, C.M., Gilles, A., David, B., Folgoas, C., Moya-Leclair, E., Kamionka, E., Desrousseaux, M.L., Texier, H., Gavalda, S., Cot, M., Guémard, E., Dalibey, M., Nomme, J., Cioci, G., Barbe, S., Chateau, M., André, I., Duquesne, S., Marty, A., 2020. An engineered PET depolymerase to break down and recycle plastic bottles. Nature 580 (7802), 216–219.

Wang, R., Wang, S., Xu, Y., Yu, X., 2020a. Engineering of a thermo-alkali-stable lipase from Rhizopus chinensis by rational design of a buried disulfide bond and combinatorial mutagenesis. J. Ind. Microbiol. Biotechnol. 47 (12), 1019–1030.

Wang, R., Wang, S., Xu, Y., Yu, X., 2020b. Enhancing the thermostability of Rhizopus chinensis lipase by rational design and MD simulations. Int. J. Biol. Macromol. 160, 1189–1200.

Xu, Z., Cen, Y.-K., Zou, S.-P., Xue, Y.-P., Zheng, Y.-G., 2019. Recent advances in the improvement of enzyme thermostability by structure modification. Crit. Rev. Biotechnol. 40 (1), 83–98.

Yang, S., Liu, M., Long, L., Zhang, R., Ding, S., 2018. Characterization of a cutinase from Myceliophthora thermophila and its application in polyester hydrolysis and deinking process. Process Biochem. 66, 106–112.

Yu, X.-W., Tan, N.-J., Xiao, R., Xu, Y., 2017. Engineering a disulfide bond in the lid hinge region of Rhizopus chinensis lipase: increased thermostability and altered acyl chain length specificity. PLoS One 7 (10), e46388.

Yves, D., Marc, K.J., Dimitri, G., Marianne, R., 2011. PoPMuSiC 2.1: a web server for the estimation of protein stability changes upon mutation and sequence optimality. BMC Bioinf. 12 (1), 151.

Zeng, W., Li, X., Yang, Y., Min, J., Huang, J.-W., Liu, W., Niu, D., Yang, X., Han, X., Zhang, L., Dai, L., Chen, C.-C., Guo, R.-T., 2022. Substrate-binding mode of a thermophilic PET hydrolase and engineering the enzyme to enhance the hydrolytic efficacy. ACS Catal. 12 (5), 3033–3040.

Zhang, L., Zhou, R., Liu, D., Zhu, M., Zhang, G., Zhang, L., Zhou, S.-F., Jiang, W., 2024. Multi-strategy orthogonal enhancement and analysis of aldo-keto reductase thermal stability. Int. J. Biol. Macromol. 264, 130691.

Zhang, Z., Lan, D., Zhou, P., Li, J., Yang, B., Wang, Y., 2016. Control of sticky deposits in wastepaper recycling with thermophilic esterase. Cellul. 24 (1), 311–321.

Zhao, T., Li, Y., Yuan, S., Ye, Y., Peng, Z., Zhou, R., Liu, J., 2020. Structure-based design of acetolactate synthase from bacillus licheniformis improved protein stability under acidic conditions. Front. Microbiol. 11.